Journal of Hazardous Materials 379 (2019) 120798

Contents lists available at ScienceDirect

Journal of Hazardous Materials

journal homepage: www.elsevier.com/locate/jhazmat

The immobilization of potentially toxic elements due to incineration and weathering of bottom ash fines

Qadeer Alam[a,*], Katrin Schollbach[a,b], Marco Rijnders[b], Corrie van Hoek[b], Sieger van der Laan[a,b], H.J.H. Brouwers[a]

[a] Department of the Built Environment, Eindhoven University of Technology, P. O. Box 513, 5600 MB, Eindhoven, the Netherlands
[b] Tata Steel, R&D, Microstructure & Surface Characterization (MSC), P. O. Box 10.000, 1970 CA, Ijmuiden, the Netherlands

GRAPHICAL ABSTRACT

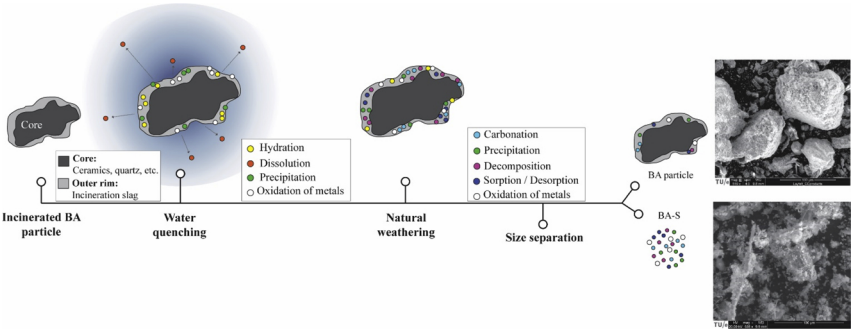

ARTICLE INFO

Keywords:
MSWI
Bottom ash
Weathering
Leaching
Potentially toxic elements

ABSTRACT

Incineration bottom ash fines (≤ 125 μm) are known to contain potentially toxic elements (PTEs) and inorganic salts. The most abundant PTEs in the fines were Zn (0.5%), Cu (0.25%), Pb (0.12%), Mn (0.08%) and Cr (0.03%). The systematic quantification of the mineral phases and PTEs associated with them was performed with a multimethod approach using quantitative XRD, phase mapping with PhAse Recognition and Characterization (PARC) software and microprobe analysis. The mineral phases in the fines can be categorized as follows: 1) residual phases (e.g., quartz), 2) incineration phases (e.g., melilitic slag and iron oxides) and 3) quenching/weathering phases (e.g., calcite, ettringite, gypsum, hydrous Fe- and Al-oxides). Among the incineration phases, the melilitic slag was observed to contain Cr, Cu and Zn with 0.02%, 0.13% and 0.19%, respectively. In order of predominance, the weathering phases containing the most PTEs were: calcite < ettringite < hydrous Al-oxides < hydrous Fe-oxides. More than 70% of the phases in the BA fines were formed during incineration and weathering processes that explain the enrichment of PTEs in the smaller particles. During the one-batch leaching test, dissolution of weathering phases, especially ettringite, was observed (total mass loss: 7.2%).

1. Introduction

The disposal of municipal solid waste (MSW) is environmentally challenging and 1.3 billion tons of MSW were generated globally in 2012 [1]. The generation of waste is expected to double by 2025 due to the increase in world population, rate of urbanization and economic

* Corresponding author.
E-mail address: q.alam@tue.nl (Q. Alam).

https://doi.org/10.1016/j.jhazmat.2019.120798
Received 29 December 2018; Received in revised form 13 June 2019; Accepted 18 June 2019
Available online 19 June 2019
0304-3894/

development, which lead to the higher consumption of resources [2]. Currently, MSW incineration in waste-to-energy plants provides an efficient way to recover energy while achieving a reduction in the mass and volume of the waste by 70% and 90%, respectively [3,4]. It produces several incineration residues, e.g., fly ash, air pollution control residues, bottom ash (BA). Among these, BA accounts for more than 80 wt.% of all the generated residues [5]. Numerous studies have explored the application potential of these ashes as a secondary raw material for making ceramics, precipitated silica, and building materials [6–9]. However, the high content of potentially toxic elements (PTEs) and inorganic salts (chlorides and sulfates) often renders these ashes unusable for recycling.

The correlation between the particle size of bottom ash and the content of contaminants (PTEs, sulfates and chlorides) is well established in the literature [10,11]. The fine particles (especially below 500 μm) are reported to contain the highest contents of the contaminants [12,13]. Therefore, the finer particles are often separated from the bigger BA fractions to obtain aggregates that fulfill the environmental legislation [14,15]. These fine particles are often enriched in weathering phases, such as calcite, ettringite, [16]. During weathering, sorption and co-precipitation of PTEs along with newly formed phases facilitate immobilization of contaminants [17]. Piantone et al. investigated the formation of secondary phases in the weathered BA along with their role in the immobilization of PTEs [18]. However, only a few phases such as calcite, iron oxides and ettringite were analyzed for PTEs contents [18]. But in order to explain leaching behavior, the quantification of all crystalline and amorphous phases along with their associated PTEs contents is required. This is a difficult task due to the complex, heterogeneous mineralogical composition of BA and the high amorphous content. For these reasons, literature regarding incineration residues is often limited to well-defined crystalline phases. The enrichment of the PTEs in the fine particles along with the mineral composition and its role in immobilization of the contaminants needs to be investigated.

This study aims to bridge this knowledge gap by investigating the origin of fine particles and their formation during the incineration and weathering processes along with mineralogy and potential to retain/release PTEs. For this purpose, a fine fraction of the BA (≤ 125 μm) was separated and its composition analyzed. Quantitative XRD was used to determine the amorphous and crystalline contents present in the fines. PhAse Recognition and Characterization (PARC) software was used for the processing of spectral imaging (SI) datasets obtained via SEM-EDX to generate phase distribution maps and the average chemical composition of the phases [19,20]. The contaminants in specific mineral phases were quantified further via electron microprobe analysis (EPMA) and the leaching potential of the fines was studied using the one-batch leaching test. Subsequently, this information was used to explain the enrichment of PTEs in the fine particles, their association with the mineral phases and their leaching behavior.

2. Materials and methods

2.1. Materials

The BA with a particle size below 4 mm, was received from Heros Sluiskil, the Netherlands, which is an incineration ash processing facility. The ashes from several municipal solid waste incinerators are treated at the company for the recycling as building materials. The fraction of BA used in this study was dry-sieved from the full fraction of BA (0–32 mm) after natural weathering of 6 weeks at the company site. In the lab, the as-received BA (≤ 4 mm) was sieved further using a vibratory sieve shaker (Retsch; AS 450 Basic) with a mesh size of 125 μm to separate the fine particles according to DIN EN 933-2. Henceforth, these size-separated fine particles will be referred to as BA-S. This study is a continuation of our previous work, in which the mineralogical composition of BA fraction with particle size below 4 mm was investigated and their immobilization potential for PTEs was assessed [16]. It was noted that the fine fraction of BA is different from the rest of the fractions and contained higher leachable contaminants. Therefore, the fine fraction (≤ 125 μm) was chosen for this study to investigate their mineralogy, origin and high leachable PTEs content.

2.2. Methods

2.2.1. Chemical analyses

The chemical composition of BA-S was determined with a X-ray fluorescence spectrometer (XRF; PANalytical Epsilon 3, standardless) using fused beads. Loss on ignition (LOI) was measured at 1000 °C until a constant mass was reached. For the preparation of fused beads, the residue from the LOI (0.95 g) was mixed with 9.5 g of borate flux, a mixture of 67% Li_2BO_7 and 33% $LiBO_2$ (Claisse). Moreover, 100 μL of 4 M LiBr was added to the mix as a non-wetting agent. The mixture was placed in a borate fluxer oven (classisse leNeo) for 24 min. at 1065 °C. For the quantification of the minor elements, multi-acid digestion (HF/HNO_3, $HClO_4$/HNO_3) was performed (Actlabs, Canada). The sample (0.25 g) was digested with hydrofluoric acid that was followed by a mixture of perchloric and nitric acids. The mixture underwent several heating and holding cycles to achieve dryness. Once the sample was dry, it was dissolved by the addition of hydrochloric and nitric acids. The digested samples were analyzed with a Perkin Elmer Sciex ELAN 6100 ICP/MS.

The X-ray diffraction pattern of the bottom ash fraction was measured with D2 from Bruker using a LynxEye detector. The radiation source was Co with $K_{\alpha1}$:1.7901 Å and $K_{\alpha2}$:1.7929 Å. For the measurement, divergence slit of 0.2° and soller slits of 2.5° were used. For the quantification of the amorphous content, 10% of Si (Siltronix, France) was added into the sample. The quantification was carried out with TOPAS 4.2 from Bruker [21]. The content of the quartz in the bottom ash sample was measured independently with a differential scanning calorimeter (DSC 822e; Mettler Toledo). The sample was heated and cooled for two consecutive cycles between 500–600 °C with a heating rate of 10 °C/min. After the two cycles, the cooling peak for the α – β conversion of quartz was quantified [22]. The content of quartz measured with the DSC was compared with the result obtained via Rietveld refinement to ensure the accuracy of the refinement.

2.2.2. Micro-analysis

The sample for SEM and EDX was prepared by mounting it in epoxy resin (Struers EpoFix). The sample was polished without the use of water and coated with carbon. The spectral imaging (SI) datasets were acquired with a SEM (JEOL JSM-7001 F) equipped with two 33 mm^2 detectors (Thermo Fisher Scientific) and NORAN-System7 hardware with NSS.3.3 software. The data acquisition was performed with a voltage of 15 kV, beam current 6.2 nA and a measurement step size of 1 μm. For two SEM image fields, a SI data set was acquired, with a 512 × 384-pixel resolution. SI datasets for two different SEM image fields of the same sample were measured, the size of a field was 512 × 384 pixel with a pixel size of 1 μm. The SI datasets were processed with PARC (PhAse Recognition, and Characterization) software, which groups the measured elemental spectra together into phases according to their chemical composition. Afterwards, these phases can be represented as colour-coded phase maps and their average composition generated [16,20].

Electron probe microanalysis (EPMA) was performed with a Cameca SX 100 microprobe. The conditions used to detect and analyze the trace elements (Cr, Ni, Cu, Zn, Sb) are as follows: accelerating voltage 15 kV, beam current 300 nA in spot mode. The peak dwell time was 240 s, background dwell time 120 s on each side of the peak. The respective detection limits under these conditions were (in ppm): Cr: 70, Ni: 90, Cu: 110, Zn: 160, Sb: 69. For the analysis of the major elements (Ca, Si, Al) a beam current of 40 nA was used. In our study, the content of Ni and Sb was below the quantification limit of the EPMA. Quantification

of the trace content of Sb in the calcium-rich matrix was not possible due to the interference from the Ca K_α line (3.690 keV) with the L_α line (3.604 keV) of Sb. Therefore, the quantification results of Ni and Sb are not reported.

2.2.3. Leaching analysis

The leaching potential of PTEs from BA-S was evaluated with the one-batch leaching test, according to EN12457-2 [23]. The sample was mixed with ultrapure deionized water in a polyethylene bottle with a liquid-to-solid ratio of 10 l/kg. The mixture was placed for the duration of 24 h on a linear reciprocating shaker (Stuart SSL2). Afterwards, the leachates were filtered and acidified with 0.2 vol.% of the HNO_3 (69%, ACS reagent grade). These leachates were analyzed for elemental composition with ICP-OES (inductively coupled plasma-optical emission spectrometer; Spectroblue from Sysmex). The contents of chlorides and sulfates in the leachates were determined with ion-chromatography (Dionex 1100), which was equipped with an ion exchange column AS9-HS (2 x 250 mm). A Na_2CO_3 (9 mM) solution with an isocratic flow of 0.25 ml/min was used as eluent. An electrolytically regenerated suppressor (Dionex AERS 500, 2 mm was used to measure suppressed conductivity for the detection of ions.

3. Results and discussions

3.1. The composition of BA fines

The chemical composition of the fine bottom ash fraction (BA-S) is provided in Table 1. In this fraction, the content of CaO is higher than the content of SiO_2, which has been reported in the literature earlier [12,24]. Furthermore, this fraction contains a high content of different PTEs (e.g., Ti, Zn, Sb, Mn and Cu) as compared to the fraction with bigger particle size [16,25,26]. The bigger fraction of BA are silica-rich and contains a lower level of potentially toxic elements [5]. The mineral composition of BA-S is given in Table 2, which shows that it contains incineration slag minerals (melilite), weathering phases (calcite, gypsum and ettringite) and high amounts of the amorphous phase. These mineral phases are frequently found in different fractions of bottom ash; however, they are rarely quantified [27–29]. The enrichment of the weathering phases in this fraction is attributed to the processing of BA. During MSW incineration, a large part of the fine particles is collected as fly ash [30]. Many of the remaining bigger particles consist of a solid core that is coated with a very inhomogeneous layer of incineration slag during incineration [31]. This BA is then subject to quenching and weathering. This can cause the complete or partial detachment of the slag layer from the core, particularly during transport and sieving [32], forming secondary fines. This process is aided by the low mechanical strength of the weathering phases themselves [33]. Therefore, BA-S (≤ 125 μm) contains large amounts of weathering products and only smaller amounts of incineration phases such as melilite. Fig. 1a and b shows the presence of many small particles, some of which are agglomerated to form larger particles. There is no clear distinction between a solid core and a layer of melilitic slag, which was reported in a previous study for ≤ 4 mm fraction of the same bottom ash [31]. Many different phases are identified via PARC, but in order to understand the chemical nature and leaching behaviour of contaminants, it is sufficient to consider only incineration and weathering phases, as they are likely to be the most reactive and contain the most contaminants.

To gain further insight into the composition and microstructure of BA-S, especially the X-ray amorphous parts, PhAse Recognition and Characterization (PARC) analysis was performed to obtain phase maps. Two different areas of the same BA-S sample were measured because the material is highly heterogeneous. Fig. 1 shows a SEM images of BA-S and their respective PARC phase maps and the overall distribution of phases, while Table 3 presents the area % of each phase and their chemical composition. Phases that could be identified as a mineral based on their composition and XRD data were named accordingly, the rest of the phases were given a name as per cement chemistry notation based on the main elements composition. These phases are expected to be X-ray amorphous because no phase with similar composition was identified with XRD analysis.

Table 1
The chemical composition of bottom ash with particle size ≤ 125 μm (BA-S). The major oxides were measured with XRF and are reported as elemental-oxides. The minor elements were measured with ICP-MS and the values are given in ppm. LOI: Loss on Ignition at 1000 °C.

Major oxides	wt.%	Major oxides	wt.%
CaO	25.0	MgO	1.7
SiO_2	19.6	P_2O_5	1.6
Al_2O_3	12.6	TiO_2	1.4
Fe_2O_3	6.3	Cl	1.2
SO_3	3.7	LOI	25.8
Minor elements	**ppm**	**Minor elements**	**ppm**
Zn	5230	Ba	115
Cu	2570	Co	70
Pb	1200	Mo	55
Mn	883	Sn	47
Cr	321	V	38
Ni	195	Cd	24
Sb	181	As	12

Table 2
The mineral composition (wt.%) based on XRD-Rietveld analysis of the original BA-S (particle size ≤ 125 μm) and the washed BA-S fraction, which was collected after the one-batch leaching test.

Minerals	BA-S	BA-S (washed)
Melilite	2.1	2.1
Feldspar	1.6	0.9
Calcite	20.3	19.0
Zeolite	1.6	1.3
Ettringite	2.5	0.3
Hematite	2.0	2.0
Apatite	4.7	3.5
Spinel	2.6	2.6
Rutile	0.3	0.5
Quartz	6.8	6.6
Gypsum	2.2	–
Halite	0.7	–
Lepidocrocite	0.8	–
Amorphous	51.9	54.1
Weight loss[a]	–	7.2
Sum	100	100

[a] The weight loss refers to the mass loss, which was observed after the one-batch leaching test.

3.2. Incineration phases

The mineral phases that are produced during incineration of MSW can be divided into iron oxides, amorphous slag and slag minerals. Hematite and magnetite (spinel) are the iron oxides that are formed out of Fe^0 (Table 2). The PTEs originating from iron oxides are most likely already present in the original Fe^0, such as Cr or Zn in coated or alloyed steel products. Incineration also creates a slag out of combustible organic and inorganic material with a sufficiently low melting point. This slag crystallizes only partially during quenching and is responsible for some of the amorphous content in BA-S. It has been reported to have a melilitic composition [28,34].

In Fig. 2a and b the distribution of slag related phases is shown. Crystalline phases that form out of this slag are typically melilite, feldspar and pyroxene [35]. Since both feldspar and pyroxene group minerals are also commonly found in nature; therefore, it is difficult to

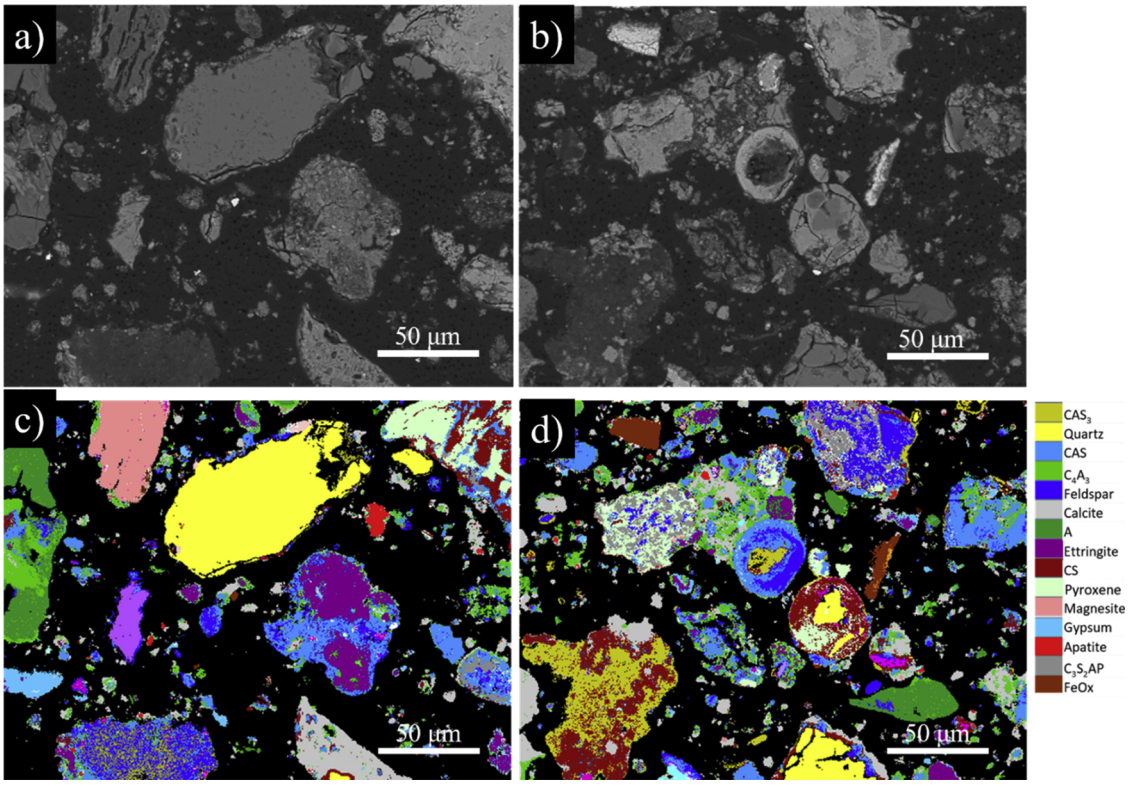

Fig. 1. SEM image of BA-S fraction with the particle size below 125 µm **a)** Field 1 and **b)** Field 2. The phase maps showing the mineral composition of the obtained via PARC analysis **c)** Field 1 and **d)** Field 2.

differentiate between their origin. However, the naturally occurring phases tend to be dense, well-defined grains that are not much affected during incineration. Feldspar and pyroxene crystallized out of slag tend to be less homogenous and intermixed with other phases. A phase rich in calcium and aluminium, C_4A_3, was also observed (Fig. 2b) that was intermixed with ettringite and calcite (Fig. 2d) and was close in composition to monosulfate ($Ca_4Al_2O_6(SO_4)\cdot 12H_2O$). This indicates the formation of C_3A during the incineration, which is a clinker mineral and has been reported in unquenched BA [26]. During the quenching process of BA, the hydration of C_3A takes place in the sulfate-rich quenching water leading to the formation of ettringite. During weathering ettringite decomposes and forms monosulfate ($Ca_4Al_2O_6(SO_4)\cdot 12H_2O$) and gypsum [29]. Due to the continued weathering, monosulfate starts carbonating and forms calcite, which can lead to the observed association of ettringite, gypsum, calcite and C_4A_3.

The chemical composition of these amorphous and crystalline slag phases is also plotted in the phase diagram of the $CaO\text{-}SiO_2\text{-}Al_2O_3$ system containing 5 wt.% MgO (Fig. 3). The sum of CaO, SiO_2 and Al_2O_3 is at least 70 wt.% of the total composition for all plotted phases. The $CaO\text{-}SiO_2\text{-}Al_2O_3$ with 5 wt.% MgO system was chosen because it represents the major oxides in BA slag phases (Table 3) and contains the phases observed via XRD and PARC. The phase diagram also shows previously reported slag phases from the ≤ 4 mm fraction of bottom ash (measured with PARC) [16,31] and completely vitrified BA (measured with EPMA) taken from the literature [27,36–38]. The phases from vitrified BA were included because there is only limited information about MSWI BA slag available. These data points fit well with the other PARC derived data points but cluster closer together because vitrified BA tends to be more homogenous than MSWI BA. Fig. 3 shows

Table 3
The chemical composition and amount (area %) of phases identified in the BA-S sample with PARC.

Mineral[a]	Phase[b]	Area %	Na_2O	MgO	Al_2O_3	SiO_2	P_2O_5	SO_3	Cl	K_2O	CaO	FeO	Others
–	A	5.1	1.9	0.1	74.2	2.8	1.1	5.5	3.2	0.7	8.0	0.7	1.7
Apatite	–	0.6	1.5	1.7	1.7	1.8	34.7	2.7	1.7	0.2	50.8	0.6	2.6
–	C_4A_3	8.6	1.4	0.6	30.3	5.3	0.7	6.3	2.1	0.6	49.0	1.3	2.3
–	CAS	14.2	1.6	1.3	26.0	29.1	1.3	3.2	1.2	1.2	29.0	3.5	2.6
–	C_3S_2AP	2.7	1.4	7.4	9.3	23.3	16.1	1.4	0.8	0.2	35.5	1.8	2.7
Pyroxene	–	5.8	0.5	14.1	6.9	45.1	1.4	0.7	0.2	0.1	24.6	3.9	2.6
–	CS	8.8	1.9	3.0	3.3	46.4	0.7	1.7	0.5	0.8	38.7	0.8	2.3
Calcite	–	13.5	0.7	0.8	4.1	3.5	0.9	3.9	0.8	0.2	82.3	0.7	2.1
Ettringite	–	5.4	0.9	0.2	17.5	5.1	0.1	30.9	1.4	0.5	41.4	0.9	1.2
Gypsum	–	1.6	0.4	0.2	2.3	1.8	0.0	55.1	1.2	0.1	37.4	0.3	1.1
FeOx	–	1.1	0.3	0.1	1.5	2.0	0.1	1.4	0.6	0.2	1.6	90.7	1.7
Quartz	–	11.5	0.0	0.0	0.0	95.1	0.0	1.5	0.1	0.0	0.0	0.1	3.2
Feldspar	–	9.0	0.5	1.4	13.3	53.7	0.5	1.7	3.6	1.3	17.5	4.2	2.2
–	CAS_3	6.5	5.2	1.8	26.8	43.0	1.0	1.6	1.0	2.9	13.0	1.7	2.1

[a] Phases that could be identified as a mineral based on their composition are given the mineral name.
[b] Unidentified phases are given a name in cement notation based on their main element contents.

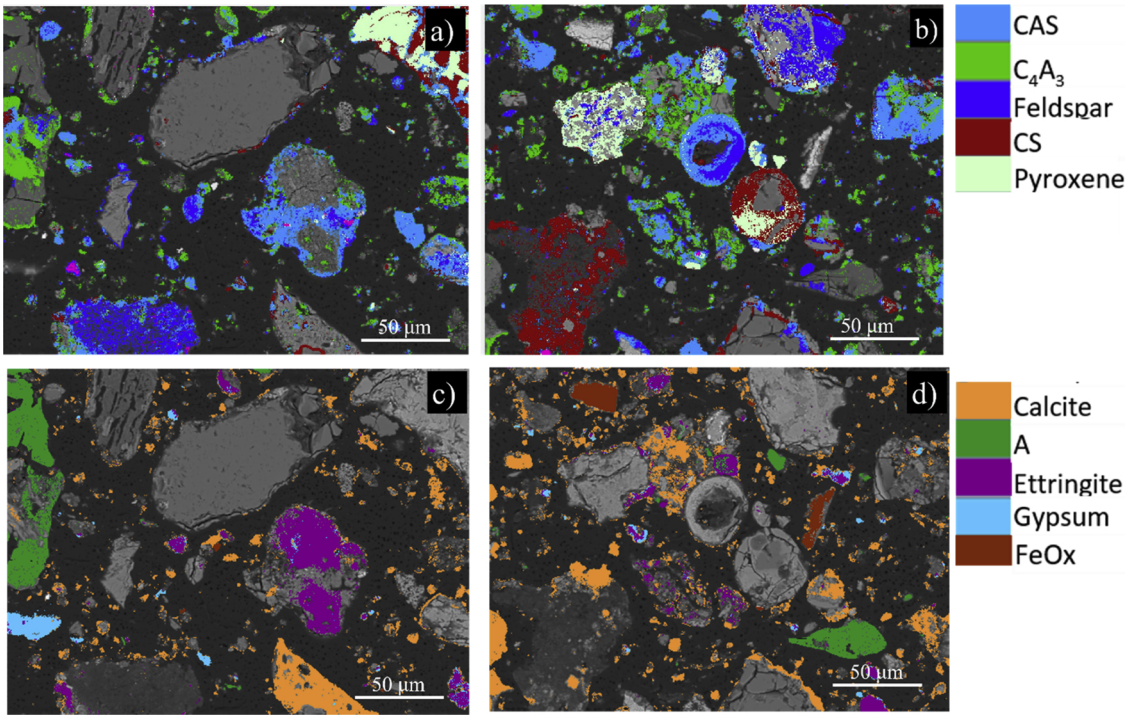

Fig. 2. Phase maps showing incineration and weathering phases from the BA-S (particle size below 125 µm). **a)** and **b)** shows only incineration slag/melt phases formed during the incineration process, **c)** and **d)** shows weathering phases that were formed after the incineration due to the carbonation and weathering processes.

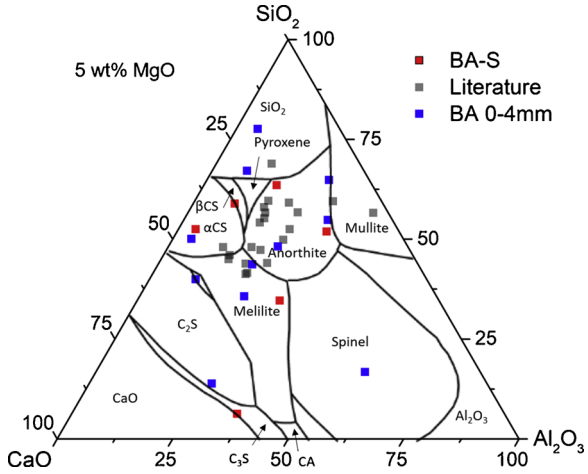

Fig. 3. The composition of the incineration slag/melt phases identified in the BA-S (particle size ≤ 125 µm) from this study, the slag phases from BA (≤4 mm) that were reported earlier [16,31] and the slag phases from the vitrified MSW [27,36–38].

that despite the extreme inhomogeneity of BA and the municipal solid waste feed, the slag phases (both amorphous and crystalline) have a similar chemical composition.

3.3. Weathering phases

The mineralogical composition of BA changes significantly during quenching and natural weathering due to numerous chemical reactions. A detailed overview of the weathering reactions taking place after the incineration is provided in Fig. 4. These reactions/processes include, but are not limited to, dissolution, oxidation/reduction metals, hydrolysis, hydration, precipitation and carbonation. During the formation of secondary phases, sorption and complexation phenomena play an important role in stabilizing the PTEs [18,32]. The enrichment and distribution of weathering phases in the BA-S fraction is evident from the PARC phase map in Fig. 2c and d. The main weathering phases in BA-S were calcite, ettringite and gypsum. Al-rich and Fe-rich phases were also observed, as shown in Fig. 2c and d, respectively. During quenching of BA, the oxidation of metals (such as Al^0) accelerates due to the alkaline pH of the quenching water and then continues during weathering due to the prevalent oxic conditions [39]. This leads to the formation of different alteration products (Aloxyhydroxides) that act as adsorbents for PTEs [40,41]. Moreover, the presence of reactive Al in combination with calcium and sulfates leads to the formation of ettringite, as shown by Eq. (1).

$$6Ca^{2+}_{(aq)} + 2Al(OH)4_{(aq)} - +3SO^{2-}_{4(aq)} + 4OH^{-}_{(aq)} + 26H_2O_{(1)} \rightarrow \underset{(Ettringite)}{3CaO{\cdot}Al_2O_3{\cdot}3CaSO_4{\cdot}32H_2O_{(s)}} \quad (1)$$

The precipitation of ettringite under these conditions leads to the immobilization of PTEs via incorporation/sorption.

Weathering of iron-rich species, such as spinel and hematite, produces hydrous iron oxides, such as lepidocrocite (γ–FeOOH) and goethite (α–FeOOH), which are the main weathering products of the iron-rich phases [42]. A small amount of lepidocrocite was also observed in the BA-S via XRD as shown in Table 2. These hydrous iron species are analogous to the aluminium hydrous species with respect to sorption of PTEs from their local environment. The role of these adsorbents in retaining PTE is often discussed and they are regarded as a source of PTEs leaching from MSWI bottom ash [43–45].

3.4. Distribution of PTEs in BA-S phases

The content of PTEs associated with the incineration and weathering phases is presented in Table 4. EPMA measurements were done on the same sample that was used for PARC mapping. The points for the electron probe microanalysis were selected using information obtained from PARC analysis. In addition to trace elements (Cr, Cu and Zn), the major elements were quantified to ensure that the correct mineral was being measured. The incineration phases, CAS and pyroxene, show a

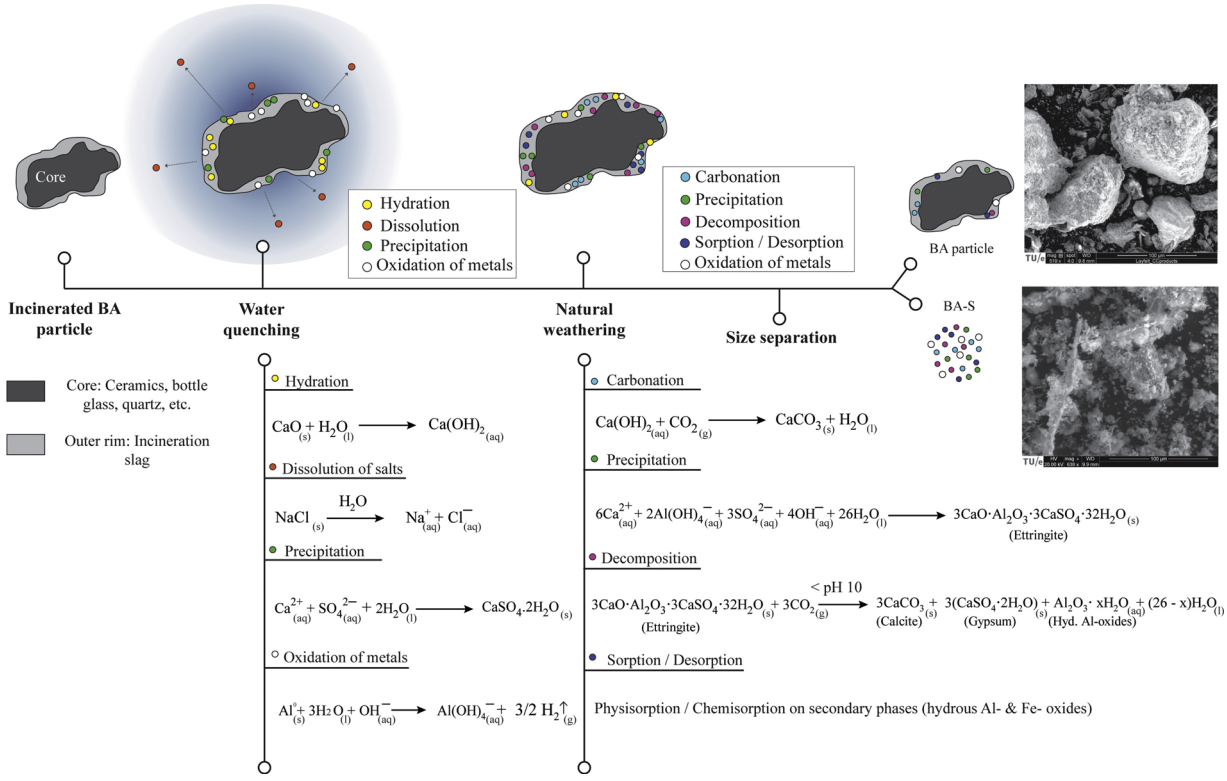

Fig. 4. Schematics showing the chemical reaction occurring during water quenching and weathering of the MSWI bottom ash.

high variation in the contents of major elements and PTEs as is evident by the high standard deviation. This is likely due to the inhomogeneous conditions during the incineration (temperature and availability of major/minor elements). The CAS phase was found to be rich in Cu and Zn with traces of Cr, while, pyroxene (which can accommodate numerous divalent and trivalent cations) showed a high content of Zn (0.48 wt.%, highest among all measured phases) in addition to minor contents of Cu and Cr.

Calcite, which is ubiquitous as a weathering phase in BA-S, can incorporate different divalent ions depending on the nature of the liquid (pH and chemical composition) percolating during the weathering of BA. The average content of Zn associated with calcite was 0.14 wt.% which is close to the previously reported value of 0.13 wt.% in calcite from MSWI bottom ash [18]. The other major weathering phase, ettringite, can also incorporate numerous ions/oxyanions [46]. In our study, two different chemical compositions of ettringite were observed with respect to the content of Cu. The Cu-rich ettringite contained 0.9 wt.% Cu, which was 15 times higher than the Cu content in the other ettringite phase. Both ettringite phases contained similar contents of Zn, while the presence of Cr and Sb was not detected to be associated with ettringite. In alkaline conditions, the prevalent chemical state of Cr and Sb is oxyanionic; chromate (CrO_4^{2-}) and antimonate ($Sb(OH)_6^-$), respectively [47]. Chromate ions could potentially replace sulfate in the structure of ettringite [46] while the proposed immobilization mechanism of antimonate is adsorption on the ettringite surface [48,49]. However, in this study, no Sb or Cr associated with ettringite phase was detected, which is likely due to the low concentrations in the bulk composition (Table 1).

The hydrous Al-oxides phase that was identified with PARC analysis is shown in Fig. 2c (labelled as A). The chemical composition of this phase shows 74.2 wt.% of Al_2O_3 (Table 3: phase A). Moreover, the PTE contents associated with the hydrous Al-oxide (Table 4) were Cr: 0.02, Cu: 0.22 and Zn 0.07 wt.%. However, it was difficult to assign a mineral phase because no crystalline Al-rich phase was identified with XRD.

Table 4
The contents major elements and trace elements (Cr, Cu and Zn) associated the mineral phases of BA-S (particle size ≤ 125 μm) measured with the electron microprobe given in wt.% (n = number of measurements, $\overline{X}$ = mean value, σ = standard deviation and L.D. = lower than detection limit).

	Calcite		Ettringite (Cu-rich)		Ettringite		CAS phase		CS phase		Pyroxene		Hyd. Al-oxides		FeO_x (Cu-rich)		FeO_x	
	(n = 4)		(n = 3)		(n = 2)		(n = 4)		(n = 3)		(n = 3)		(n = 3)		(n = 3)		(n = 4)	
	$\overline{X}$	σ	$\overline{X}$	σ	$\overline{X}$	σ	$\overline{X}$	σ	$\overline{X}$	σ	$\overline{X}$	σ	$\overline{X}$	σ	$\overline{X}$	σ	$\overline{X}$	σ
Major elements																		
Ca	39.5	1.0	25.1	5.2	21.8	0.9	13.4	5.7	31.1	0.07	16.6	6.4	6.3	1.7	2.49	0.9	0.9	0.03
Si	4.0	3.0	2.4	0.1	10.8	0.8	8.5	1.8	22.8	0.18	13.5	6.0	1.1	0.2	1.02	0.4	0.5	0.12
Al	1.9	0.8	8.7	2.0	9.0	3.2	8.5	2.0	1.3	0.54	1.4	0.8	32.3	0.1	0.92	0.5	0.3	0.08
Fe	–	–	–	–	–	–	–	–	–	–	–	–	–	–	4.63	1.5	43.4	3.25
Trace metals																		
Cr	L.D.	–	L.D.	–	L.D.	–	0.02	0.01	L.D.	–	0.09	0.07	0.02	0.01	0.021	0.01	0.026	0.01
Cu	0.06	0.02	0.88	0.49	0.06	0.01	0.13	0.08	0.028	0.001	0.05	0.02	0.22	0.12	0.313	0.08	0.066	0.03
Zn	0.14	0.05	0.13	0.01	0.19	0.03	0.19	0.13	0.026	0.002	0.48	0.04	0.07	0.02	0.113	0.04	0.174	0.06

Table 5
The leaching of BA-S (particle size ≤ 125 µm) obtained via a one-batch leaching test and its comparison with the legal limits (Dutch Soil Quality decree) [50]. The percent of the total amount of PTEs present that were leached during the g test is given as percent leachable. The values are given in ppm and were normalized for the dry mass of residues. L.D: lower than the detection limit.

Parameters	Legal limits[a]	BA-S	Percent leachable (%)
Ba	22	L.D	–
Cr	0.63	1.20	0.37
Cu	0.9	6.61	0.26
Mo	1	1.12	2.04
Sb	0.32	0.97	0.54
As	0.9	0.16	1.33
Cd	0.04	L.D	–
Co	0.54	0.05	0.21
Pb	2.3	L.D	–
Ni	0.44	0.07	0.04
Se	0.15	L.D	–
Sn	0.4	L.D	–
V	1.8	0.16	0.42
Zn	4.5	0.47	0.01
Cl^-	616	11136	92.80
SO_4^{2-}	1730	20097	–
pH	–	10.8	–

[a] Legal leaching limits for contaminants measured according to column leaching test (NEN 7383:2004) for use as non-shaped building materials.

Most likely this PARC phase represents X-ray amorphous aluminium oxyhydroxides. Furthermore, the Fe-rich phases identified with PARC are given in Fig. 2d. These phases can also be divided into two groups based on the Cu content, as shown in Table 4. FeO_x (Cu-rich) contained approximately 5 times more Cu than the other FeO_x phase. As discussed earlier (section 3.2.), the speciation of FeO_x cannot be resolved via PARC or electron microprobe analysis. Therefore, it is unclear if the PTEs are associated with hematite or spinel, both of which can accommodate divalent and trivalent PTE ions (Cu^{2+}, Zn^{2+} and Cr^{3+}) in their crystal structure. Alternatively, this phase could be a hydrous Fe-oxide (such as lepidocrocite) that can adsorb multiple ionic species on its surface.

3.5. Leaching behaviour

The chemical composition of the leachates obtained from the BA-S via one-batch leaching test is presented in Table 5. The leaching of the PTEs was compared with their respective legal limits as prescribed by the Dutch Soil Quality Decree (SQD) [50]. In this fraction of bottom ash, the contents of Cu, Mo, Cr and Sb were higher than the legal threshold, which is common for BA [32,40,51]. Furthermore, this fraction contained high amounts of leachable sulfates and chlorides.

The mineralogical transformations of BA-S due to the one-batch leaching test were evaluated with quantitative XRD. The original mineral composition of BAS was compared with the washed residues and is provided in Table 2. The mass loss due to the leaching test was measured and accounted for 7.2 wt.%. Almost complete dissolution of ettringite and gypsum was observed. Moreover, a minor amount of calcite (1.3 wt.%) was dissolved as expected considering the low solubility of calcite in alkaline medium (pH 10.8) releasing only a minor amount of the Zn and Cu. The dissolution of ettringite and gypsum also contributed to the release of Cu and Zn into the leachates. The leachates also contain other PTEs (Cr, Sb and Mo) which were above their legal threshold. In our study, Cr was found to be associated with the incineration phases (CAS, pyroxene and FeO_x) and hydrous aluminum oxides. The dissolution of the amorphous melilitic slag (CAS) is expected in the leachates and could contribute to the Cr concentration. Meanwhile, hydrous metal oxides immobilize PTEs via sorption and the release of these sorbed species is expected during the leaching test, contributing to the PTE content. However, due to the amorphous nature of these phases, it is challenging to quantify their degree of dissolution. The Rietveld quantification also indicated an increase in amorphous content of BA-S by 2 wt.% after the one-batch leaching test indicating the formation of new amorphous phases.

The leaching results in combination with EMPA confirm that the formation of weathering phases in BA reduces the leaching of PTEs for short to mid-term; however, these weathering phases are stable only in a limited pH range. For example, the decomposition of ettringite can be triggered by a pH decrease, as shown by Eq. (2).

$$\underset{(Ettringite)}{3CaO\cdot Al_2O_3\cdot 3CaSO_4\cdot 32H_2O_{(s)}} + 3CO_{2(g)} \xrightarrow{pH<10} \underset{(Calcite)}{3CaCo_{3(s)}} + \underset{(Gypsum)}{3(CaSO_4\cdot 2H_2O)_{(s)}} + \underset{(Hyd.Al\text{-}oxides)}{Al_2O_3\cdot xH_2O_{(aq)}} + (26-x)H_2O_{(l)} \quad (2)$$

The decomposition products of this reaction include gypsum, calcite and hydrous Al-oxides [52].

Generally, this decrease in the pH from 12 to 8 is a consequence of long-term weathering in which carbonation reactions take place. Similarly, in earlier studies, leaching of Cr and Sb is reported to increase after six months of weathering treatment due to the decrease in pH because of the carbonation and weathering reactions [48,53]. Therefore, the immobilization of PTEs due to the formation of weathering products and their long-term stability need to be carefully considered while designing treatments for these residues.

4. Conclusions and implications

4.1. Conclusions

BA is a complex heterogeneous material, but its understanding can be simplified by focusing its incineration slag and weathering products. The key findings of this study are as follows:

- The fine particles of BA are composed of smaller amounts of incineration phases (melilitic slag, pyroxene and iron oxides) and large amounts of secondary weathering products (calcite, ettringite, gypsum, zeolite and hydrous metal oxide) that account for more than 70% of the fines.
- The phases formed during incineration are mainly amorphous and accommodate the trace elements present in the environment during incineration. In our case, these slag phases contained all investigated PTEs (Cr, Cu and Zn).
- The PTE content of the weathering phases was as follows: calcite < ettringite < hydrous Al-oxides < hydrous Fe-oxides. The hydrous oxides of Al and Fe were detected via PARC and XRD, respectively. They can play an important role in the sorption of PTEs from their local environment and contain significant amounts of Cr, Cu and Zn.
- After the one-batch leaching test, the mass loss of the BA fines was 7.2 wt.%. mainly due to the dissolution of gypsum and ettringite releasing the Cu and Zn associated with them into the solution. Moreover, the leachable Cr likely originated from the hydrous metallic oxides of Fe and Al.

4.2. Implications

The sorption and co-precipitation of PTEs with incineration and weathering phases plays an important role in their immobilization and the leaching potential of PTEs is correlated with the chemical stability of the respective phase. For example, the ettringite phase in BA-S contained both Cu and Zn. Due to weathering, the pH of BA can drop below 10 triggering the decomposition of ettringite, which leads to the leaching of Cu and Zn after long term weathering process.

The incineration phases, especially the amorphous incineration slag

with a melilitic composition, can react in an alkaline environment, thus releasing PTEs. If the fines are used in Portland cement, which generates a high pH during hydration, they could also contribute to strength development. However, the content of gypsum and ettringite can delay the early hydration of Portland cement. This could be countered by using cement with lower sulfate content along with BA fines.

MSWI bottom ashes can be successfully recycled as building materials if the most contaminated fractions, particles below 500 µm, are separated during the treatment processes. Another way to improve the environmental properties of the ashes would be using a dry-quenching method, in which ashes are cooled down in a dry or semi-dry environment.

Acknowledgements

The authors would like to acknowledge the financial support provided by NWO (Nederlandse Organisatie voor Wetenschappelijk Onderzoek), the Netherlands, under the project number 10019729: “Environmental concrete based on the treated MSWI bottom ashes”. Special thanks to V. Caprai for designing the schematics presented in Fig. 4 of this manuscript.

References

[1] P. Bhada-Tata, D.A. Hoornweg, What a Waste? A Global Review of Solid Waste Management, (2012) Washington, DC, http://documents.worldbank.org/curated/en/302341468126264791/What-a-waste-a-global-review-of-solid-waste-management . (Accessed 14 December 2018).

[2] D. Hoornweg, P. Bhada-Tata, C. Kennedy, Environment: waste production must peak this century, Nature 502 (2013) 615–617, https://doi.org/10.1038/502615a.

[3] J. Yao, W.-B.B. Li, M. Tang, C.-R.R. Fang, H.-J.J. Feng, D.-S.S. Shen, Effect of weathering treatment on the fractionation and leaching behavior of copper in municipal solid waste incinerator bottom ash, Chemosphere 81 (2010) 571–576, https://doi.org/10.1016/j.chemosphere.2010.08.038.

[4] P. Tang, M.V.A. Florea, P. Spiesz, H.J.H. Brouwers, Characteristics and application potential of municipal solid waste incineration (MSWI) bottom ashes from two waste-to-energy plants, Constr. Build. Mater. 83 (2015) 77–94, https://doi.org/10.1016/j.conbuildmat.2015.02.033.

[5] C.C. Wiles, Municipal solid waste combustion ash: state-of-the-knowledge, J. Hazard. Mater. 47 (1996) 325–344, https://doi.org/10.1016/0304-3894(95)00120-4.

[6] V. Caprai, K. Schollbach, H.J.H. Brouwers, Influence of hydrothermal treatment on the mechanical and environmental performances of mortars including MSWI bottom ash, Waste Manage. 78 (2018) 639–648, https://doi.org/10.1016/J.WASMAN.2018.06.030.

[7] D. Dabo, R. Badreddine, L. De Windt, I. Drouadaine, Ten-year chemical evolution of leachate and municipal solid waste incineration bottom ash used in a test road site, J. Hazard. Mater. 172 (2009) 904–913, https://doi.org/10.1016/j.jhazmat.2009.07.083.

[8] A. Bourtsalas, L.J. Vandeperre, S.M. Grimes, N. Themelis, C.R. Cheeseman, Production of pyroxene ceramics from the fine fraction of incinerator bottom ash, Waste Manage. 45 (2015) 217–225, https://doi.org/10.1016/j.wasman.2015.02.016.

[9] Q. Alam, Y. Hendrix, L. Thijs, A. Lazaro, K. Schollbach, H.J.H. Brouwers, Novel low temperature synthesis of sodium silicate and ordered mesoporous silica from incineration bottom ash, J. Clean. Prod. 211 (2019) 874–883, https://doi.org/10.1016/J.JCLEPRO.2018.11.173.

[10] J.M. Chimenos, A.I. Fernández, L. Miralles, M. Segarra, F. Espiell, Short-term natural weathering of MSWI bottom ash as a function of particle size, Waste Manage. 23 (2003) 887–895, https://doi.org/10.1016/S0956-053X(03)00074-6.

[11] R. del Valle-Zermeño, J. Gómez-Manrique, J. Giro-Paloma, J. Formosa, J.M. Chimenos, Material characterization of the MSWI bottom ash as a function of particle size. Effects of glass recycling over time, Sci. Total Environ. 581–582 (2017) 897–905, https://doi.org/10.1016/J.SCITOTENV.2017.01.047.

[12] S. Yang, A. Saffarzadeh, T. Shimaoka, T. Kawano, Existence of Cl in municipal solid waste incineration bottom ash and dechlorination effect of thermal treatment, J. Hazard. Mater. 267 (2014) 214–220, https://doi.org/10.1016/j.jhazmat.2013.12.045.

[13] Q. Alam, M.V.A. Florea, K. Schollbach, H.J.H. Brouwers, A two-stage treatment for Municipal Solid Waste Incineration (MSWI) bottom ash to remove agglomerated fine particles and leachable contaminants, Waste Manage. 67 (2017) 181–192, https://doi.org/10.1016/J.WASMAN.2017.05.029.

[14] Q. Alam, K. Schollbach, M.V.A. Florea, H.J.H. Brouwers, Investigating washing treatment to minimize leaching of chlorides and heavy metals from MSWI bottom ash, 4th Int. Conf. Sustain. Solid Waste Manage. (2016), http://uest.ntua.gr/cyprus2016/proceedings/proceedings.html.

[15] O. Holm, E. Wollik, T. Johanna Bley, Recovery of copper from small grain size fractions of municipal solid waste incineration bottom ash by means of density separation, Int. J. Sustain. Eng. 7038 (2017) 1–11, https://doi.org/10.1080/19397038.2017.1355415.

[16] Q. Alam, K. Schollbach, C. van Hoek, S. van der Laan, T. de Wolf, H.J.H. Brouwers, In-depth mineralogical quantification of MSWI bottom ash phases and their association with potentially toxic elements, Waste Manage. 87 (2019) 1–12, https://doi.org/10.1016/J.WASMAN.2019.01.031.

[17] T. Sabbas, A. Polettini, R. Pomi, T. Astrup, O. Hjelmar, P. Mostbauer, G. Cappai, G. Magel, S. Salhofer, C. Speiser, S. Heuss-Assbichler, R. Klein, P. Lechner, Management of municipal solid waste incineration residues, Waste Manage. 23 (2003) 61–88, https://doi.org/10.1016/S0956-053X(02)00161-7.

[18] P. Piantone, F. Bodénan, L. Chatelet-Snidaro, Mineralogical study of secondary mineral phases from weathered MSWI bottom ash: implications for the modelling and trapping of heavy metals, Appl. Geochem. 19 (2004) 1891–1904, https://doi.org/10.1016/j.apgeochem.2004.05.006.

[19] C.J.G. van Hoek, M. de Roo, G. van der Veer, S.R. van der Laan, A SEM-EDS study of cultural heritage objects with interpretation of constituents and their distribution using PARC data analysis, Microsc. Microanal. 17 (2011) 656–660, https://doi.org/10.1017/S1431927610094390.

[20] C.J.G. van Hoek, J. Small, S.R. van der Laan, Large area phase mapping using PhAse Recognition and Characterization (PARC) software, Micros. Today 24 (2016), https://doi.org/10.1017/S1551929516000572.

[21] A.A. Coelho, *TOPAS* and *TOPAS-Academic*: an optimization program integrating computer algebra and crystallographic objects written in C++, J. Appl. Crystallogr. 51 (2018) 210–218, https://doi.org/10.1107/S1600576718000183.

[22] Y. Hendrix, Q. Alam, L. Thijs, A. Lazaro, H.J.H. Brouwers, Green synthesis of waterglass from municipal solid waste incineration bottom ash, 9th Int. Symp. Cem. Concr. (ISCC 2017) (2017) 1–4 http://www.iscc2017.org.cn.

[23] J. Holm, J.B. Hansen, CEN EN 12457 Leaching Test : Comparison of Test Results Obtained by Part 1 and 2 with Test Results Obtained by Part 3 Dorthe Lærke Baun Jesper Holm Jette Bjerre Hansen Margareta Wahlström, (2003).

[24] D. Bendz, P.L. Tüchsen, T.H. Christensen, The dissolution kinetics of major elements in municipal solid waste incineration bottom ash particles, J. Contam. Hydrol. 94 (2007) 178–194, https://doi.org/10.1016/j.jconhyd.2007.05.010.

[25] S. Yang, A. Saffarzadeh, T. Shimaoka, T. Kawano, Y. Kakuta, The impact of thermal treatment and cooling methods on municipal solid waste incineration bottom ash with an emphasis on Cl, Environ. Technol. 37 (2016) 1–8, https://doi.org/10.1080/09593330.2016.1155651.

[26] K. Inkaew, A. Saffarzadeh, T. Shimaoka, Modeling the formation of the quench product in municipal solid waste incineration (MSWI) bottom ash, Waste Manage. 52 (2016) 159–168, https://doi.org/10.1016/j.wasman.2016.03.019.

[27] A.P. Bayuseno, W.W. Schmahl, Understanding the chemical and mineralogical properties of the inorganic portion of MSWI bottom ash, Waste Manage. 30 (2010) 1509–1520, https://doi.org/10.1016/j.wasman.2010.03.010.

[28] J.D. Eusden, T.T. Eighmy, K. Hockert, E. Holland, K. Marsella, Petrogenesis of municipal solid waste combustion bottom ash, Appl. Geochem. 14 (1999) 1073–1091, https://doi.org/10.1016/S0883-2927(99)00005-0.

[29] Y. Wei, T. Shimaoka, A. Saffarzadeh, F. Takahashi, Mineralogical characterization of municipal solid waste incineration bottom ash with an emphasis on heavy metal-bearing phases, J. Hazard. Mater. 187 (2011) 534–543, https://doi.org/10.1016/j.jhazmat.2011.01.070.

[30] C.H.K. Lam, A.W.M. Ip, J.P. Barford, G. McKay, Use of incineration MSW ash: a review, Sustainability 2 (2010) 1943–1968, https://doi.org/10.3390/su2071943.

[31] K. Schollbach, Q. Alam, V. Caprai, M.V.A. Florea, S.R. Van der Laan, C.J.G. van Hoek, H.J.H. Brouwers, Combined chracterization of the MSWI bottom ash, Proc. Thirty-Eighth Int. Conf. Cem. Microsc. (2016) 74–84.

[32] A. Saffarzadeh, T. Shimaoka, Y. Wei, K.H. Gardner, C.N. Musselman, Impacts of natural weathering on the transformation/neoformation processes in landfilled MSWI bottom ash: a geoenvironmental perspective, Waste Manage. 31 (2011) 2440–2454, https://doi.org/10.1016/j.wasman.2011.07.017.

[33] J.W. Anthony, R.A. Bideaux, K.W. Bladh, M.C. Nichols, Handbook of Mineralogy, Mineralogical Society of America, Chantilly, VA 20151-1110, USA, 2003http://www.handbookofmineralogy.org/.

[34] N.M. Piatak, M.B. Parsons, R.R.S II, Characteristics and environmental aspects of slag: a review, Appl. Geochem. 57 (2015) 236–266, https://doi.org/10.1016/j.apgeochem.2014.04.009.

[35] V.D. Eisenhüttenleute, M. Allibert, Slag Atlas, Verlag Stahleisen, 1995.

[36] A. Saffarzadeh, T. Shimaoka, Y. Motomura, K. Watanabe, Chemical and mineralogical evaluation of slag products derived from the pyrolysis/melting treatment of MSW, Waste Manage. 26 (2006) 1443–1452, https://doi.org/10.1016/J.WASMAN.2005.12.005.

[37] A. Saffarzadeh, T. Shimaoka, Y. Motomura, K. Watanabe, Petrogenetic characteristics of molten slag from the pyrolysis/melting treatment of MSW, Waste Manage. 29 (2009) 1103–1113, https://doi.org/10.1016/J.WASMAN.2008.08.008.

[38] A. Saffarzadeh, T. Shimaoka, Y. Motomura, K. Watanabe, Characterization study of heavy metal-bearing phases in MSW slag, J. Hazard. Mater. 164 (2009) 829–834, https://doi.org/10.1016/J.JHAZMAT.2008.08.093.

[39] D. Xuan, C.S. Poon, Removal of metallic Al and Al/Zn alloys in MSWI bottom ash by alkaline treatment, J. Hazard. Mater. 344 (2018) 73–80, https://doi.org/10.1016/J.JHAZMAT.2017.10.002.

[40] G. Cornelis, T. Van Gerven, C. Vandecasteele, Antimony leaching from uncarbonated and carbonated MSWI bottom ash, J. Hazard. Mater. 137 (2006) 1284–1292, https://doi.org/10.1016/j.jhazmat.2006.04.048.

[41] R.M. Santos, G. Mertens, M. Salman, Ö. Cizer, T. Van Gerven, Comparative study of ageing, heat treatment and accelerated carbonation for stabilization of municipal solid waste incineration bottom ash in view of reducing regulated heavy metal/

metalloid leaching, J. Environ. Manage. 128 (2013) 807–821, https://doi.org/10.1016/J.JENVMAN.2013.06.033.
[42] Y. Wei, T. Shimaoka, A. Saffarzadeh, F. Takahashi, Alteration of municipal solid waste incineration bottom ash focusing on the evolution of iron-rich constituents, Waste Manage. 31 (2011) 1992–2000, https://doi.org/10.1016/J.WASMAN.2011.04.021.
[43] Jeannet A. Meima, R.N.J. Comans, Application of surface complexation/precipitation modeling to contaminant leaching from weathered municipal solid waste incinerator bottom ash, Environ. Sci. Technol. 32 (1998) 688–693, https://doi.org/10.1021/ES9701624.
[44] J.J. Dijkstra, J.C.L. Meeussen, H.A. Van der Sloot, R.N.J. Comans, A consistent geochemical modelling approach for the leaching and reactive transport of major and trace elements in MSWI bottom ash, Appl. Geochem. 23 (2008) 1544–1562, https://doi.org/10.1016/J.APGEOCHEM.2007.12.032.
[45] D.S. Apul, K.H. Gardner, T.T. Eighmy, A.-M. Fällman, R.N.J. Comans, Simultaneous application of dissolution/precipitation and surface complexation/surface precipitation modeling to contaminant leaching, Environ. Sci. Technol. 39 (2005) 5736–5741, https://doi.org/10.1021/ES0486521.
[46] H. Pollmann, Mineralisation of Wastes and Industrial Residues, Shaker Verlag, Aachen, 2010.
[47] G. Cornelis, C.A. Johnson, T. Van Gerven, C. Vandecasteele, Leaching mechanisms of oxyanionic metalloid and metal species in alkaline solid wastes: a review, Appl. Geochem. 23 (2008) 955–976, https://doi.org/10.1016/j.apgeochem.2008.02.001.
[48] J. Van Caneghem, B. Verbinnen, G. Cornelis, J. de Wijs, R. Mulder, P. Billen, C. Vandecasteele, Immobilization of antimony in waste-to-energy bottom ash by addition of calcium and iron containing additives, Waste Manage. 54 (2016) 162–168, https://doi.org/10.1016/j.wasman.2016.05.007.
[49] G. Cornelis, T. Van Gerven, C. Vandecasteele, Antimony leaching from MSWI bottom ash: modelling of the effect of pH and carbonation, Waste Manage. 32 (2012) 278–286, https://doi.org/10.1016/j.wasman.2011.09.018.
[50] Soil Quality Decree, Regeling Bodemkwaliteit, VROM, Ruimte en Milieu, Ministerie van Volkshuisvesting, Ruimtelijke Ordeling en Milieubeheer, Den Haag, 2007.
[51] H. Lassesson, K.K. Fedje, B.-M. Steenari, Leaching for recovery of copper from municipal solid waste incineration fly ash: influence of ash properties and metal speciation, Waste Manage. Res. 32 (2014) 755–762, https://doi.org/10.1177/0734242X14542147.
[52] S.C.B. Myneni, S.J. Traina, T.J. Logan, Ettringite solubility and geochemistry of the Ca(OH)2–Al2(SO4)3–H2O system at 1 atm pressure and 298 K, Chem. Geol. 148 (1998) 1–19, https://doi.org/10.1016/S0009-2541(97)00128-9.
[53] D. Blanc, L. Gonzalez, M. Lupsea-Toader, C. de Brauer, Mineralogical evolution and leaching behaviour of a heap of bottom ash as a function of time: influence on its valorization, Waste Biomass Valoriz. (2018) 1–11, https://doi.org/10.1007/s12649-018-0444-1.